3B2v8.06a/w (Dec 5 2003).51c +model | CAGEO : 1646 | Prod.Type:FTP pp.1–9(col.fig.:6,8,9) | ED:BibhuPrasad PAGN:Kaushik SCAN:Manjula

ARTICLE IN PRESS

ELSEVIER

Computers & Geosciences ▮ (▮▮▮▮) ▮▮▮–▮▮▮

COMPUTERS & GEOSCIENCES

www.elsevier.com/locate/cageo

Numerical modeling of submarine mass-movement generated waves using RANS model

D. Yuk[a], S.C. Yim[a,*], P.L.-F. Liu[b]

[a]Department of Civil Engineering, Oregon State University, Corvallis, OR, USA
[b]School of Civil and Environmental Engineering, Cornell University, Ithaca, NY, USA

Received 31 October 2003; accepted 26 October 2005

Abstract

In this paper a numerical model for predicting waves generated by nearshore submarine mass-movements is described. The model is based on the Reynolds averaged Navier–Stokes (RANS) equations with the $k-\varepsilon$ turbulence model. The volume of fluid (VOF) method is employed to track the free surface. Numerical results obtained from the present model are validated with laboratory experiments and analytical solutions. Very good agreements are observed for both submarine and aerial mass movements. Numerical experiments are performed to obtain the empirical formula for the maximum runup and rundown as functions of slide properties.

Keywords: Submarine mass movement; Numerical model; Turbulence; Breaking waves

1. Introduction

Motivated by the needs for preservation of human lives and coastal infrastructure, and for the deployment and operation of special structural and mechanical systems in coastal areas, the study of nearshore wave motions and wave–structure interaction has been of interest to coastal scientists and engineers for many years.

Coastal wave generation due to submarine mass movement is a complex process. While the length scale of a submarine mass movement is usually smaller than that of a seafloor displacement created by a fault rupture, the time-scale is usually longer. Therefore, the concept of "initial free surface displacement" in the wave generation region becomes a critical issue. Hence the evolution of the free surface displacement in the source region of mass movement needs to be modeled entirely. Furthermore, the characteristics of a submarine mass movement, including the soil properties, volume and area of the mass movement, also require a post-event bathymetry survey.

Several numerical models have been developed to describe the waves generated by submerged or aerial mass movements. With the common assumption that the geometry and the time history of the mass movement can be prescribed, these models adopt various additional approximations in hydrodynamics. For instance, Lynett and Liu (2002) presented a model based on the depth-integrated nonlinear wave equations, which include the frequency dispersion effects. Therefore, their model

*Corresponding author.
E-mail address: Solomon.Yim@oregonstate.edu (S.C. Yim).

0098-3004/$ - see front matter
doi:10.1016/j.cageo.2005.10.028

can simulate relatively short waves that might be generated by a submarine mass movement. Grilli and Watts (1999) adopted a boundary integral equation method (BIEM), based on the potential flow theory, and developed a fully nonlinear model for mass movement-generated waves. However, the approach does not take into account wave breaking, which could be important in the vicinity of the generation region as well as the runup region. The depth-averaged model suffers the same drawback as the BIEM model in terms of the lack of capability of modeling breaking waves. However, it is much more computationally efficient as it has reduced the 3D problem to a 2D problem in the horizontal space. Heinrich (1992) modified the NASA-VOF2D model, which is a 2D (vertical plane) nonlinear free surface model based on the Navier–Stokes equations, to study the generation, propagation and runup of tsunamis created by landslides. The effects of turbulence are not considered. Heinrich compared his numerical results for both submarine and aerial mass movements with his own experiments. The agreement is reasonable, except in the regions where wave-breaking-induced turbulence is important.

In recent years, significant advancement in modeling wave-breaking process and interactions between breaking waves and coastal structures has been made. For example, Cornell breaking waves and structures model (COBRAS) is based on the Reynolds Averaged Navier–Stokes (RANS) equations with a $k-\varepsilon$ turbulence closure model. While a nonlinear Reynolds stress model is employed to allow anisotropic turbulence, the volume of fluid (VOF) method is used to track the free surface movements. COBRAS has been verified and validated by comparing numerical results with experimental data for runup and rundown of breaking waves on a uniform beach (Lin and Liu, 1998a,b; Lin et al., 1999). It also has the capability of simulating wave–structure interactions, where the structures are rigid, stationary, fully submerged or surface piercing (Hsu et al., 2002).

The primary goal of this paper is to modify COBRAS to allow time-dependent moving solid boundaries such that mass movement-created waves can be simulated. Since COBRAS is capable of calculating turbulence, the modified model will be able to simulate breaking waves, runup and rundown. Here, we shall first present briefly the theoretical background of COBRAS and discuss the necessary modification to simulate the mass movement. 2D numerical results are then compared with experimental data. Some discussions on the future extensions are given at the end of the paper.

2. Description of the model

In this section the mathematical formulation and the associated numerical algorithm of COBRAS are discussed briefly. More detailed discussions can be found in Lin and Liu (1998 a, b). The model is based on the RANS equations. For a turbulent flow, the velocity field and pressure field can be decomposed into two parts: the mean (ensemble average) velocity and pressure $\langle u_i \rangle$ and $\langle p \rangle$, and the deviatoric (or turbulent) velocity and pressure u_i' and p'. Thus, $u_i = \langle u_i \rangle + u_i'$ and $p = \langle p \rangle + p'$ in which $i = 1, 2, 3$ for a 3D flow. If the fluid is assumed incompressible, the mean flow field is governed by the RANs equations:

$$\frac{\partial \langle u_i \rangle}{\partial x_i} = 0, \tag{1}$$

$$\frac{\partial \langle u_i \rangle}{\partial t} + \langle u_j \rangle \frac{\partial \langle u_i \rangle}{\partial x_j} = -\frac{1}{\rho}\frac{\partial \langle p \rangle}{\partial x_i} + g_i + \frac{1}{\rho}\frac{\partial \langle \tau_{ij} \rangle}{\partial x_j} - \frac{\partial \langle u_i' u_j' \rangle}{\partial x_j} \tag{2}$$

in which ρ is the density of the fluid, g_i the ith component of the gravitational acceleration, and the mean molecular stress tensor $\langle \tau_{ij} \rangle = 2\mu \langle \sigma_{ij} \rangle$ with μ, the molecular viscosity and $\langle \sigma_{ij} \rangle$, the rate of strain tensor of the mean flow. In the momentum equation (2), the influence of the turbulent fluctuations on the mean flow field is represented by the Reynolds stress tensor $-\rho \langle u_i' u_j' \rangle$. Many second-order turbulence closure models have been developed for different applications. In the present model, the Reynolds stress is approximated by a nonlinear algebraic stress model:

$$\rho \langle u_i' u_j' \rangle = \frac{2}{3}\rho k \delta_{ij} - C_d \frac{k^2}{\varepsilon}\left(\frac{\partial \langle u_i \rangle}{\partial x_j} + \frac{\partial \langle u_j \rangle}{\partial x_i}\right) - \rho \frac{k^3}{\varepsilon^2}\left[\begin{array}{c} C_1 \left(\begin{array}{c} \frac{\partial \langle u_i \rangle}{\partial x_l}\frac{\partial \langle u_l \rangle}{\partial x_j} + \frac{\partial \langle u_j \rangle}{\partial x_l}\frac{\partial \langle u_l \rangle}{\partial x_i} \\ -\frac{2}{3}\frac{\partial \langle u_l \rangle}{\partial x_k}\frac{\partial \langle u_k \rangle}{\partial x_l}\delta_{ij} \end{array}\right) \\ + C_2 \left(\frac{\partial \langle u_i \rangle}{\partial x_k}\frac{\partial \langle u_j \rangle}{\partial x_k} - \frac{1}{3}\frac{\partial \langle u_l \rangle}{\partial x_k}\frac{\partial \langle u_l \rangle}{\partial x_k}\delta_{ij}\right) \\ + C_3 \left(\frac{\partial \langle u_k \rangle}{\partial x_i}\frac{\partial \langle u_k \rangle}{\partial x_j} - \frac{1}{3}\frac{\partial \langle u_l \rangle}{\partial x_k}\frac{\partial \langle u_l \rangle}{\partial x_k}\delta_{ij}\right) \end{array}\right] \tag{3}$$

in which C_d, C_1, C_2 and C_3 are empirical coefficients, δ_{ij} the Kronecker delta, $k = \langle u_i' u_i' \rangle / 2$ the turbulent kinetic energy, and $\varepsilon = \nu \langle (\partial u_i' / \partial x_j)^2 \rangle$ the dissipation rate of turbulent kinetic energy, where $\nu = \mu/\rho$ is the molecular kinematic viscosity. It is noted that for the conventional eddy viscosity model $C_1 = C_2 = C_3 = 0$ in (3) and the eddy viscosity is then expressed as $\nu_t = C_d k^2/\varepsilon$. Compared with the conventional eddy viscosity model, the nonlinear Reynolds stress model (3) can be applied to general anisotropic turbulent flows.

The governing equations for k and ε are modeled as (Lin and Liu, 1998a, b)

$$\frac{\partial k}{\partial t} + \langle u_j \rangle \frac{\partial k}{\partial x_j} = \frac{\partial}{\partial x_j}\left[\left(\frac{\nu_t}{\sigma_k} + \nu\right)\frac{\partial k}{\partial x_j}\right] - \langle u_i' u_j' \rangle \frac{\partial \langle u_i \rangle}{\partial x_j} - \varepsilon, \tag{4}$$

$$\frac{\partial \varepsilon}{\partial t} + \langle u_j \rangle \frac{\partial \varepsilon}{\partial x_j} = \frac{\partial}{\partial x_j}\left[\left(\frac{\nu_t}{\sigma_k} + \nu\right)\frac{\partial \varepsilon}{\partial x_j}\right] + C_{1\varepsilon}\frac{\varepsilon}{k}\nu_t\left(\frac{\partial \langle u_i \rangle}{\partial x_j} + \frac{\partial \langle u_j \rangle}{\partial x}\right)\frac{\partial \langle u_i \rangle}{\partial x_j} - C_{2\varepsilon}\frac{\varepsilon^2}{k} \tag{5}$$

in which σ_k, σ_ε, $C_{1\varepsilon}$ and $C_{2\varepsilon}$, are empirical coefficients. The coefficients in Eqs. (3)–(5) have been determined by performing many simple experiments and enforcing the physical realizability; the recommended values for these coefficients can be found in Lin and Liu (1998a, b).

Appropriate boundary conditions need to be specified. For the mean flow field, both the no-slip and the free-slip boundary condition can be imposed on the solid boundary. Along the mass surface, the velocity of the moving boundary is either prescribed or determined by dynamic equilibrium of the mass. The zero-stress condition is required on the mean free surface by neglecting the effect of airflow. For the turbulent field, near the solid boundary, the log–law distribution of mean tangential velocity in the turbulent boundary layer is applied so that the values of k and ε can be expressed as functions of distance from the boundary and the mean tangential velocity outside the viscous sublayer. On the free surface, the zero-gradient boundary conditions are imposed for both k and ε, i.e., $\partial k/\partial n = \partial \varepsilon/\partial n = 0$. A low level of k for the initial and inflow boundary conditions is assumed.

In the numerical model, the RANS equations are solved by a finite difference two-step projection method. The forward time difference method is used to discretize the time derivative. The advection terms are discretized by the combination of central difference method and upwind method. The central difference method is employed to discretize the pressure gradient terms as well as stress gradient terms. The VOF method is used to track the free surface. The transport equations for k and ε are solved with the similar method used in solving the momentum equations (Lin and Liu, 1998a, b).

3. Numerical results and discussions

To validate the numerical model, numerical simulations of several laboratory experiments have been carried out, including waves generated by vertical bottom movements (Hammack, 1973) and by a sliding triangular block on a uniform beach (Heinrich, 1992). In Hammack's experiments waves do not break in the generation region and the present numerical results agree with Hammack's data very well. In this paper we shall focus our discussion on Heinrich's experiments in which the generated waves break.

The computational domain is 12 m in x-direction and 2 m in y-direction. A variable grid size system is used in the x-direction with minimum grid size of 0.01 m and a fixed grid size of 0.01 m is employed in y-direction. To satisfy all stability conditions and restrictions of the incorporated methods, a fixed time step of 5×10^{-4} s is used. Numerical results in generation (i.e., near moving mass) and propagation regions are compared with experimental data as shown in Figs. 1 and 2. The submarine mass movement is modeled by a triangular shaped moving boundary that is initially located at 0.01 m below the free surface as in Heinrich (1992). The measured displacement time history from the Heinrich experiment is used as prescribed motion of the triangular mass. Since the grid size is not small enough to resolve the boundary layer, the free-slip boundary condition is applied on all the solid boundaries including sliding body, slopes, and channel bottom. As shown in Figs. 1 and 2, wave profiles in the generation region and the propagation region are in good agreement with experimental data. However, some deviations are observed in wave profile at $t = 1.5$ s when the reflected wave starts to break. It is surmised that the disagreement in wave profile is caused by the random nature of turbulence near wave breaking where the "exact" measured value is difficult to determine.

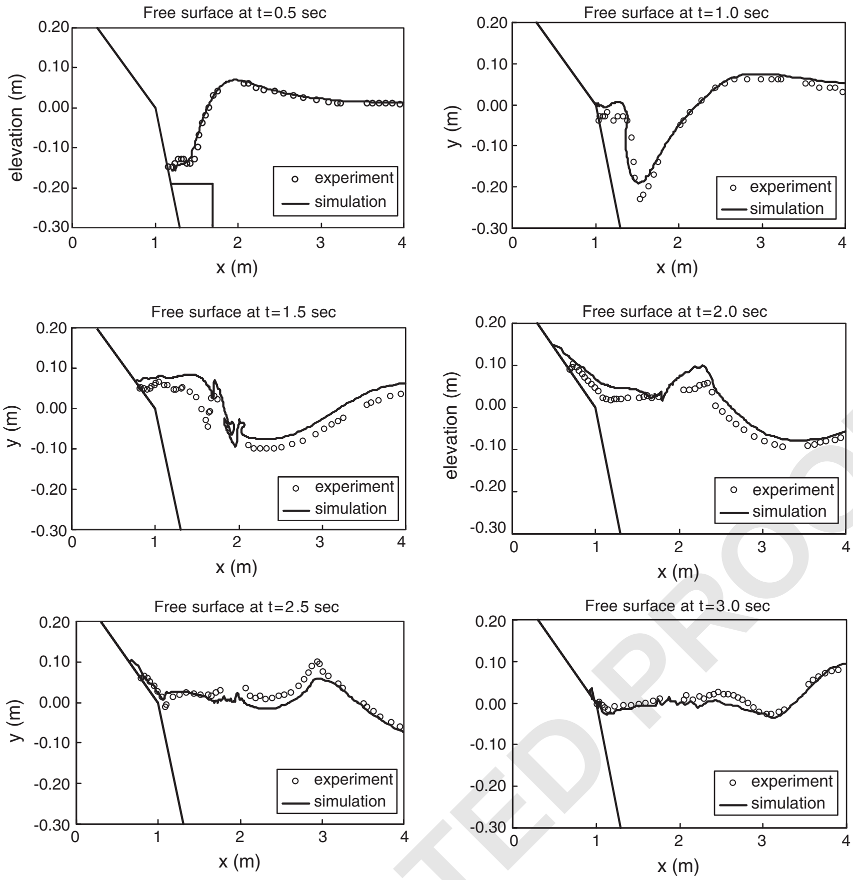

Fig. 1. Free-surface comparisons between simulation and experimental data at 0.5, 1.0, 1.5, 2.0, 2.5, and 3.0 s in wave generation region. First panel shows portion of triangular shape moving boundary.

A convergence test using minimum grid sizes of 0.005, 0.01, 0.02, and 0.04 m has been performed. A fine grid of 30 cells is used to resolve maximum wave height. It is observed that convergence is achieved with a grid size 0.01 m. This value (or smaller) is employed throughout the study.

Turbulence generation by the submarine mass movement on a beach and its evolution are examined. Fig. 3 shows the contours of turbulence intensity at $t = 0.5, 1.0, 1.5, 2.0, 2.5,$ and 3.0 s. It is observed that when the mass is in motion turbulence is generated around the upper right corner because of flow separation. Once the waves generated by the moving mass reach shore, waves are reflected. After the mass movement stops, turbulence is generated by the breaking of the reflected wave near the free surface and turbulence intensity decreases gradually. The maximum turbulence intensity can reach 0.83 m/s, which is almost 50% of the mean velocity.

The influence of the submarine mass movement velocity is examined by varying the displacement time history. Denoting by a_0 as the initial acceleration of the mass movement measured in the experiment, we have calculated three additional cases with accelerations that are $0.5a_0$, $0.75a_0$ and $1.25a_0$, respectively. In these simulations the total displacement and the volume of mass movement remain constant so that only one parameter, i.e., velocity of the moving mass, is varied. The effects of mass movement velocity on maximum wave heights, runup and rundown are shown in Figs. 4 and 5, respectively. As expected, the magnitudes of the wave height, runup and rundown increase with increasing acceleration.

Another case examined is an aerial slide in which a part of the moving body is initially located above the free surface and slides down along a uniform slope. Therefore, the moving solid boundary intersects the free surface until the moving body is

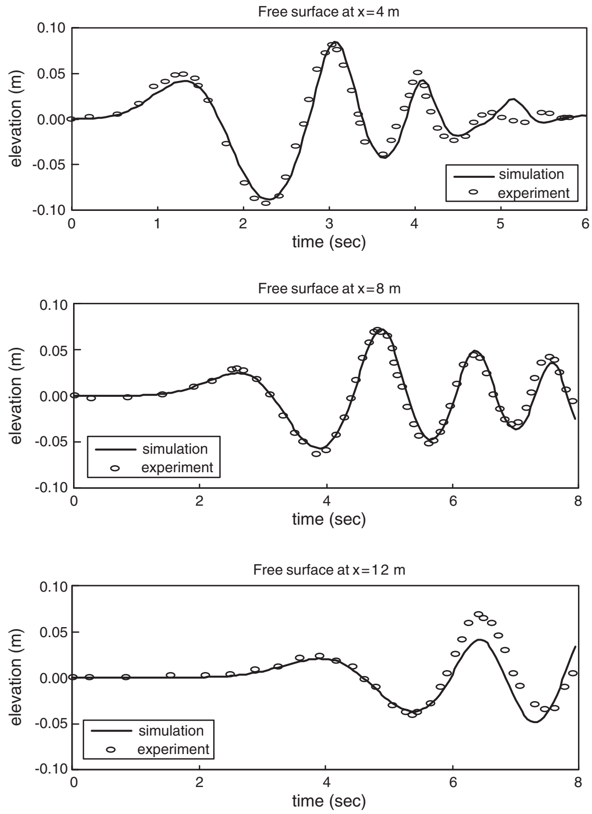

Fig. 2. Free-surface comparisons between simulation and experimental data at $x = 4, 8$, and 12 m in propagation region.

completely submerged. During this period of time, a special treatment in the VOF function is required to satisfy the law of mass conservation. This is necessary because the pressure in the free surface cell is not calculated from the Poisson pressure equation, and is specified by the free surface boundary condition. Thus, a source/sink term cannot be used in the free surface and the moving boundary interface cell to generate an equal amount of fluid corresponding to the volume change due to the moving boundary. An algorithm to treat the free surface and moving-boundary interface cell is developed and incorporated in the code.

Numerical simulations are performed and compared with the experimental data obtained by Heinrich (1992) to validate the predictive capability of the numerical model for an aerial sliding. The problem setup is exactly the same as that for the submarine slide except that the moving body is located initially just above the free surface. Wave profiles in the generation region at $t = 0.6, 1.0$, and 1.5 s are compared with experimental data as shown in Fig. 6. From the wave profile at $t = 0.6$ s, we observe that the wave starts to break and becomes highly random. The discrepancy of wave profiles at $t = 1.5$ s might be attributed to turbulence.

The numerical model developed in this study is utilized to investigate the functional relationship between both the runup and rundown of submarine slide generated waves and the geometric parameters of the sliding body and slope. From the previous work by Chen (2002), the following form of functional relation is employed.

$$\frac{\eta_{rd}}{b} = c_0 \gamma^{c_1} \left(\frac{A_l}{A_w}\right)^{c_2} (\sin\theta)^{c_3} (\sin\beta)^{c_4}, \tag{6}$$

$$\frac{\eta_{up}}{b} = d_0 \gamma^{d_1} \left(\frac{A_l}{A_w}\right)^{d_2} (\sin\theta)^{d_3} (\sin\beta)^{d_4}. \tag{7}$$

In the above equation, c_0, c_1, c_2, c_3, c_4, d_0, d_1, d_2, d_3, and d_4 are constants to be determined, η_{rd} the maximum rundown, η_{up} the maximum runup, b the base length of triangular sliding body, θ the slope angle, γ the specific weight of sliding body, β the angle of top face of sliding body, A_l the area of sliding body, and A_w the area of fluid above the sliding body. A series of numerical experiments is conducted to examine the functional relations.

In previous studies (Chen, 2002; Grilli and Watts, 1999) of functional relations between submarine slide and runup/rundown, the motion of sliding body is determined by solving the differential equation obtained by balancing inertial, added mass, gravitational, buoyancy, and fluid dynamic drag forces. In this study, the sliding body movement is not predetermined but obtained by considering the instantaneous dynamic equilibrium of the moving body including the coupled fluid–structure interaction. An iterative procedure is introduced to compute the sliding body movement. For the parametric study of maximum runup and rundown presented in this study, no prescribed sliding body motion is used because there is no experimental data available. Details of the fluid–-structure interaction modeling will be presented in a future paper. The numerical results shown in Fig. 1 are obtained by using predetermined time history of sliding block. The time history of sliding block measured from the experiment conducted by Heinrich (1991) is used for sliding block motion in that particular simulation.

For the numerical experiments for runup and rundown, the computational domain is discretized

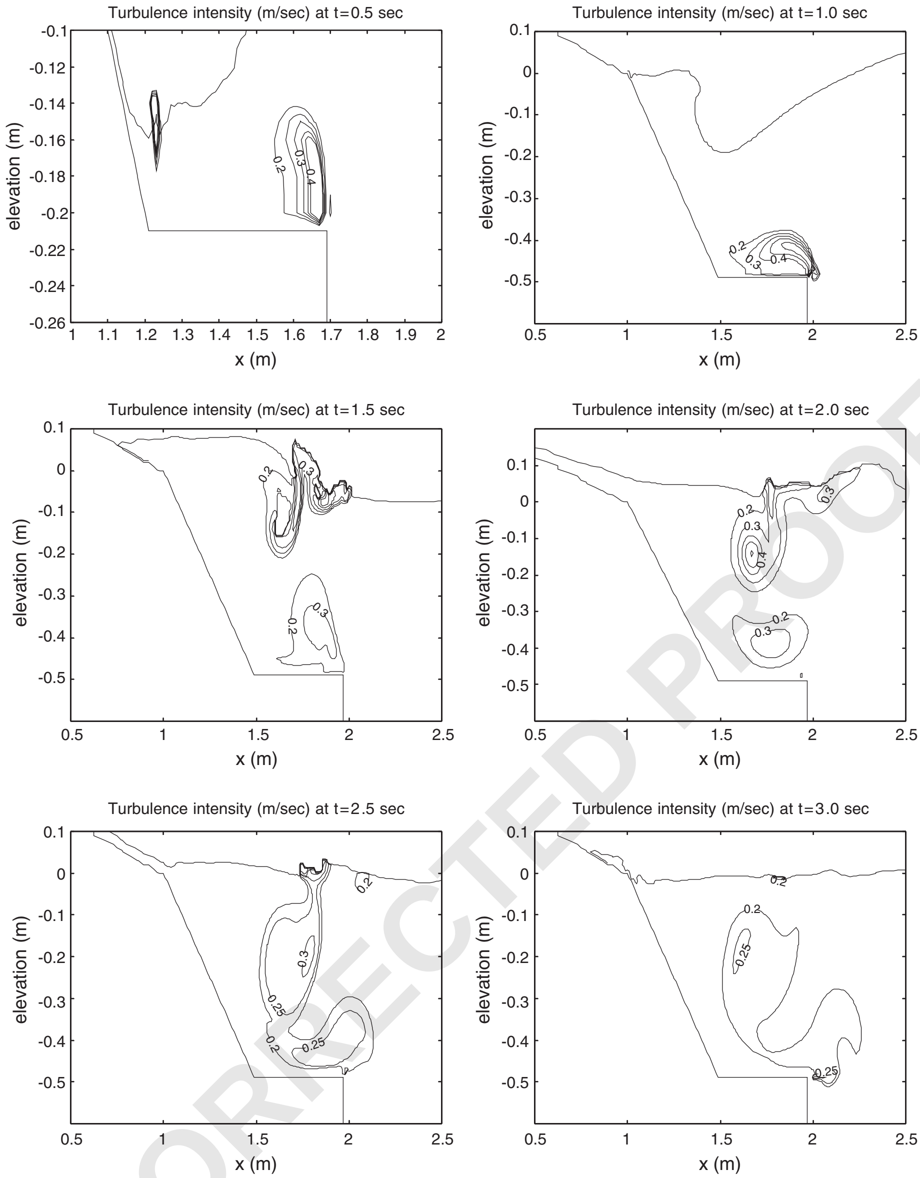

Fig. 3. Turbulence intensity around moving body at $t = 0.5, 1.0, 1.5, 2.0, 2.5$, and $3.0\,\mathrm{s}$.

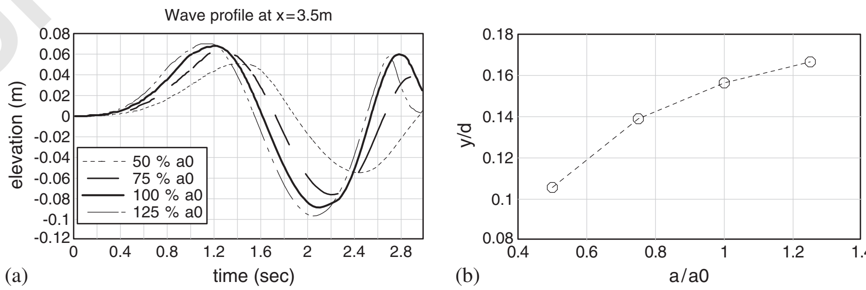

Fig. 4. Influence of sliding mass velocity on wave height: (a) time series of free surface at $x = 3.5\,\mathrm{m}$, and (b) maximum wave height.

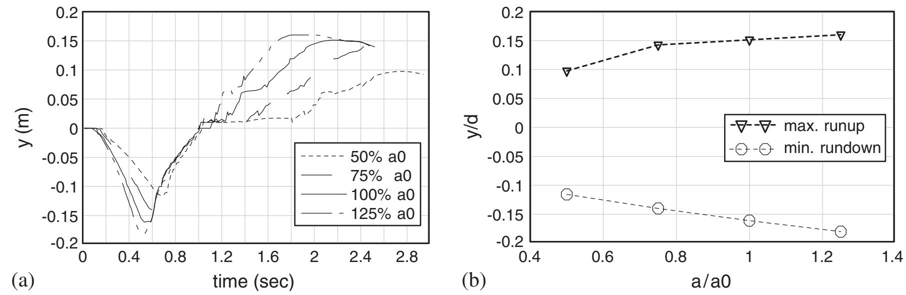

Fig. 5. Influence of mass movement velocity on runup and rundown: (a) elevation of free surface level along solid fixed boundary, and (b) maximum and minimum free surface level.

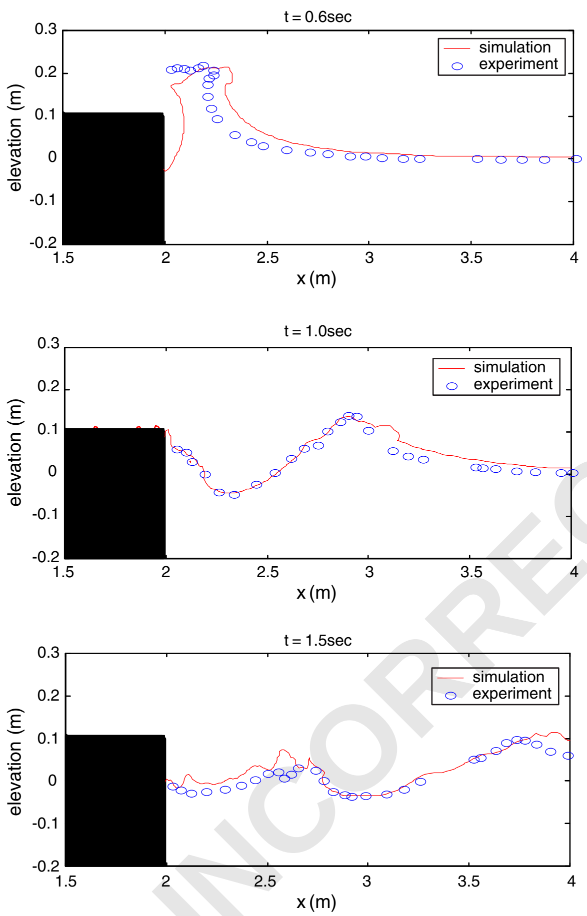

Fig. 6. Free surface comparisons between simulation and experimental data at 0.5, 1.0, and 1.5 s in wave generation region. Solid rectangles shows upper right corner of triangular shape moving boundary.

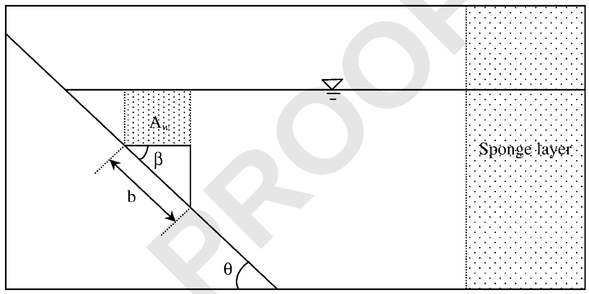

Fig. 7. Computational domain and numerical experiment setup.

by 410 × 280 grids points in horizontal and vertical direction, respectively, and variable time step is used to advance solutions in time so that stability conditions are satisfied. The slope where landslides occur and runup/rundown is measured is located on the left end of computational domain. In addition to specifying the domain boundary at the right edge as "open", a sponge layer of sufficient width is placed on the right side to prevent reflections of waves at domain boundary and ensure full energy absorption (see Fig. 7).

Four sets of numerical experiments are conducted. In each set, only one parameter is varied with all others being fixed so that the effects of varying the particular parameter can be examined. The parameter space used in this study is shown in Table 1. The range of parameter variation is determined by considering the possibility of physical realization. For example, the specific density of landslides can be less than 1.0, but physically it may not be realizable because of the buoyant force.

To measure the runup and rundown, numerical wave gauges are placed along the slope. However, maximum and minimum vertical elevations of the free surface on the slope are recorded as runup and rundown, respectively. The distance that waves move along the slope can also be calculated using the maximum and minimum values in the vertical direction and the slope angle.

Figs. 8 and 9 show the effects of parameters considered in this study on rundown/runup and the

Table 1
Parameters used for runup and rundown simulations

Test	$\sin\theta$	γ	β	A_l	A_w	A_l/A_w	$\sin\beta$
1	0.707	1.4	1.0	0.250	0.240	1.0399	0.707
2	0.707	1.8	1.0	0.250	0.240	1.0399	0.707
3	0.707	2.0	1.0	0.250	0.240	1.0399	0.707
4	0.707	2.4	1.0	0.250	0.240	1.0399	0.707
5	0.707	2.8	1.0	0.250	0.240	1.0399	0.707
6	0.707	2.12	0.707	0.125	0.071	1.768	0.707
7	0.707	2.12	0.707	0.125	0.115	1.083	0.707
8	0.707	2.12	0.707	0.125	0.145	0.865	0.707
9	0.707	2.12	0.707	0.125	0.180	0.695	0.707
10	0.707	2.12	0.707	0.125	0.212	0.589	0.707
11	0.707	2.12	0.707	0.125	0.248	0.505	0.707
12	0.707	2.0	1.0	0.25	0.311	2.24	0.985
13	0.707	2.0	1.0	0.25	0.311	2.24	0.966
14	0.707	2.0	1.0	0.25	0.311	2.24	0.940
15	0.707	2.0	1.0	0.25	0.311	2.24	0.866
16	0.707	2.0	1.0	0.25	0.24	1.040	0.707
17	0.643	2.0	1.0	0.25	0.24	1.040	0.707
18	0.574	2.0	1.0	0.25	0.24	1.040	0.707
19	0.500	2.0	1.0	0.25	0.24	1.040	0.707
20	0.423	2.0	1.0	0.25	0.24	1.040	0.707
21	0.342	2.0	1.0	0.25	0.24	1.040	0.707

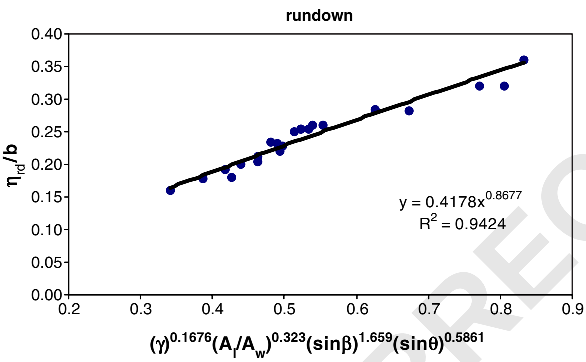

Fig. 8. Least-squares fit of rundown to numerical simulation data.

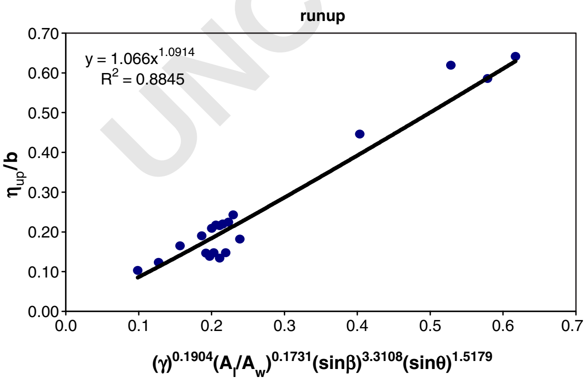

Fig. 9. Least-squares fit of runup to numerical simulation data.

results of regression analysis. The power curves used to fit the data ensure that runup and rundown do not occur when any of parameters are zero. In determining the final formula for runup and rundown, the power curves are used again and the exponents from curve fit are multiplied to obtain the coefficients for final runup and rundown formula.

Based on the numerical results shown in Figs. 8 and 9, the functional relationships between runup/rundown and the parameters are found to be

$$\frac{\eta_{rd}}{b} = 0.4178\gamma^{0.1454}\left(\frac{A_l}{A_w}\right)^{0.2803}(\sin\beta)^{1.4395}(\sin\theta)^{0.5086}, \tag{8}$$

$$\frac{\eta_{up}}{b} = 1.0593\gamma^{0.2078}\left(\frac{A_l}{A_w}\right)^{0.1889}(\sin\beta)^{3.6134}(\sin\theta)^{1.6566}. \tag{9}$$

Note that larger runup and rundown are observed as expected for increasing mass density, face angle, slope angle, and decreasing initial submergence of the landslide.

4. Concluding remarks

The capability and accuracy of the present numerical model in predicting wave generation by submarine and aerial mass movements and propagation has been validated. In addition, the influence of moving body velocity on runup and rundown has been examined. For the higher sliding body velocity, maximum runup and rundown are increased as expected.

Turbulence generation by triangular shape moving body occurs around the upper right corner due to flow separation and near the free surface where waves break. Careful experiments measuring the velocity field are desirable to validate the prediction of the turbulence intensity.

Relationships between maximum runup and maximum rundown as functions of specific density, initial submergence level, angle of the moving mass as well as slope angle are identified. The runup and rundown formulae show good agreement with physical intuitions.

Finally we should remark that the present results are limited to 2D slides, which are uniform along the shoreline. In reality slides are 3D. The predicted maximum runup based on the present 2D slides might not be conservative. In the case of a 3D slide, additional lateral (in the alongshore direction) as well as the on-offshore waves can be generated due to the free surface drawdown and rebound above the moving slide. This feature requires further study.

Acknowledgements

Partial support from the National Science Foundation Grants CMS-9908392 and CMS-0217744, and the US Office of Naval Research Grants N00014-92-1221, N00014-97-1-0581, and N00014-04-10008 are gratefully acknowledged.

References

Chen, Y.-Y., 2002. Numerical modeling of 2D waves generated by submarine landslides. M.S. Thesis, Cornell University, Ithaca, NY.

Grilli, S.T., Watts, P., 1999. Modeling of waves generated by a moving submerged body. Applications to underwater landslides. Engineering Analysis Boundary Elements 23, 645–656.

Hammack, J.L., 1973. A note on tsunamis: their generation and propagation in an ocean of uniform depth. Journal of Fluid Mechanics 60, 769–799.

Heinrich, P., 1992. Nonlinear water waves generated by submarine and aerial landslides. Journal of Waterway, Port, Coastal and Ocean Engineering, ASCE 118, 249–266.

Hsu, T.-J., Sakakiyama, T., Liu, P.L.-F., 2002. Validation of a model for wave-structure interactions. Coastal Engineering 46, 25–50.

Lin, P., Liu, P.L.-F., 1998a. A numerical study of breaking waves in the surf zone. Journal of Fluid Mechanics 359, 239–264.

Lin, P., Liu, P.L.-F., 1998b. Turbulence transport, vorticity dynamics, and solute mixing under plunging breaking waves in surf zone. Journal of Geophysical Research 103, 15677–15694.

Lin, P., Chang, K.-A., Liu, P.L.-F., 1999. Runup and rundown of solitary waves on sloping beaches. Journal of Waterway, Port, Coastal and Ocean Engineering, ASCE 125 (5), 247–255.

Lynett, P.J., Liu, P.L.-F., 2002. A numerical study of submerged landslide generated waves and runup. Proceedings of the Royal Society A 458, 2885–2910.